Photovoltaic Charge Generation in Organic Semiconductors Based on Long-Range Energy Transfer

David C. Coffey, Andrew J. Ferguson, Nikos Kopidakis, and Garry Rumbles*

Chemical and Material Sciences Center, National Renewable Energy Laboratory (NREL), 1617 Cole Boulevard, Golden, Colorado 80401

ARTICLE

ABSTRACT For efficient charge generation in organic solar cells, photogenerated excitons must migrate to a donor/acceptor interface where they can be dissociated. This migration is traditionally presumed to be based on diffusion through the absorber material. Herein we study an alternative migration route—two-step exciton dissociation—whereby the exciton jumps from the donor to acceptor before charge creation takes place. We study this process in a series of multilayer donor/barrier/acceptor samples, where either poly(3-hexylthiophene) (P3HT) or copper phthalocyanine (CuPc) is the donor, fullerene (C_{60}) is the acceptor, and *N*,*N*-diphenyl-*N*,*N*-bis(3-methylphenyl)-[1,1-bisphenyl]-4,4-diamine (TPD) acts as a barrier to energy transfer. By varying the thickness of the barrier layer, we find that energy transfer from P3HT to C_{60} proceeds over large distances (~50% probability of transfer across a 11 nm barrier), and that this process is consistent with long-range Förster resonance energy transfer (FRET). Finally, we demonstrate a fundamentally different architecture concept that utilizes the two-step mechanism to enhance performance in a series of P3HT/CuPc/C_{60} devices.

KEYWORDS: solar cell · energy transfer · charge transfer · Förster · FRET · organic semiconductor · photovoltaic · microwave conductivity

Combinations of conjugated polymers, small molecules, and semiconducting quantum dots make promising materials for use in low-cost solar cells.[1,2] Predicting how new combinations will perform has proved challenging, however, as seemingly well-matched mixtures often fail to photogenerate charge effectively. In the standard description of how these "excitonic" solar cells convert photons into free charge, light absorption produces strongly-bound singlet excitons that must diffuse to a type-II heterojunction (donor/acceptor interface) with energy offsets sufficient to dissociate the excitons into free charge.[1,3] When material combinations providing a suitable type-II heterojunction fail to perform, explanations such as poor device morphology and poor charge transport can sometimes explain the failure, but not always. Indeed it is becoming apparent that the standard description does not account for the full complexity of the charge-generation process.[4−9] The existence of multiple charge-generating pathways in excitonic solar cells is becoming increasingly evident, and the ability to understand and predict these multiple pathways has become an important goal.

One key step in the process of charge generation in organic photovoltaics is exciton migration from an absorber material to a donor/acceptor interface. Measurements of semiconducting polymers typically find an exciton migration range of ~5−10 nm.[10−13] Since ~100 nm thick films are necessary for good light absorption, donor and acceptor materials are commonly mixed to create a bulk heterojunction whereby a donor/acceptor interface is always accessible within an exciton's migration length.[1,14] While this material blending improves charge generation, it simultaneously leads to disordered charge transport pathways that inhibit charge extraction. Thus improved charge creation comes at the expense of charge transport. One strategy to move beyond this limiting paradigm would be to significantly enhance the range of exciton migration.

Exciton migration in organic materials is commonly described as a diffusive process based on an exciton hopping model. Individual hops are understood in the language of Förster resonance energy transfer (FRET) theory, where an emitter and an absorber exchange energy through long-range dipole−dipole interactions.[1,15−19] Biology provides a prime example of where exciton migration does not limit performance. In the photosynthetic reaction center, excitons generated in an array of more than the 200 absorbing pigments diffuse with near perfect efficiency across the array to a single acceptor.[20,21] In contrast, organic photovoltaics (OPVs) must compensate for poor energy transport by utilizing nanoscale mixing

*Address correspondence to garry.rumbles@nrel.gov.

Received for review May 19, 2010 and accepted August 06, 2010.

Published online August 24, 2010.
10.1021/nn101106b

(which hinders charge transport) and optically thin devices (which hinder light absorption). As such, while internal quantum efficiencies of today's organic photovoltaics (OPVs) can reach ~100%, external quantum efficiencies (EQE) rarely surpass 60%.[22,23] Theoretical simulations suggest that exciton diffusion lengths an order of magnitude larger than experimentally measured might be accessible in organic materials by reducing defects and material disorder.[17,24] However, there has been small progress achieving such gains in polymer systems, and poor energy migration continues to limit today's devices.

Recent studies suggest alternative routes to charge generation are also accessible in organic semiconductors. In the standard description of charge generation, a singlet exciton must first diffuse to a donor/acceptor interface. The dissociation event of an exciton at this interface is commonly assigned to a one-step process whereby an electron (hole) is transferred from the donor (acceptor) to the acceptor (donor). The charge transfer process is thought to occur on a subpicosecond time scale, while the reverse reaction is kinetically hindered.[25] However, numerous departures from this standard description have been reported. Several groups have determined that charged polarons are produced with up to a 30% yield in poly(3-hexylthiophene) (P3HT) films without any corresponding acceptor material.[26−28] Other groups have demonstrated that singlet excitons can progress through long-lived triplet exciton states that only later dissociate into free charge.[28,29] Further, and underlying our research, several groups have shown that a two-step dissociation process can occur in some material combinations, whereby a singlet exciton generated in the donor, for example, does not simply diffuse to a donor/acceptor interface, but rather energy transfers from the donor to the acceptor (step one), and then dissociates by hole transfer back to the donor (step two).[5−7,30]

Photoluminescence spectra and photoluminescence decay measurements have been used to determine that the first step in the two-step process can and does occur—FRET from an absorber across the donor/acceptor interface to the acceptor.[5−7,31] A more recent study by Lloyd *et al.* showed that the two-step mechanism likely occurs in polymer−fullerene devices and contributes to the overall efficiency, possibly significantly.[30] To reach this conclusion in P3HT/C_{60} bilayer devices, they deposited a 2.5 nm layer of *N*,*N*-bis(3-methylphenyl)-*N*,*N*-diphenylbenzidene (TPD) between the P3HT and C_{60}. This TPD layer blocks the "standard" exciton dissociation based on electron transfer from the P3HT to C_{60} while retaining the possibility of two-step exciton dissociation. The resulting P3HT/TPD/C_{60} devices achieved efficiencies similar to standard P3HT/C_{60} devices, indicating that the two-step process is probably an important route for charge generation in P3HT/fullerene devices. However, the length scale of the energy transfer step in the two-step process was not explored, nor has the two-step process been explicitly utilized to improve device performance in polymer or small-molecule OPVs.

RESULTS AND DISCUSSION

Herein, we investigate the two-step exciton dissociation process in greater detail: employing time-resolved microwave conductivity (TRMC), UV−vis absorption measurements, photovoltaic device characterization, and EQE measurements. We have extended upon previous studies of the two-step mechanism by probing the range of the energy transfer process. We accomplish this by fabricating a series of multilayer films and devices with interlayers of varying thickness that block one-step charge generation but permit two-step charge generation. By increasing the interlayer thickness, we probe the distance over which the energy transfer process must occur. In each experiment, we use TRMC to identify the active charge-generation interfaces. Finally, we fabricate multilayer devices to illustrate how the two-step mechanism can be used to supplement device performance. These device data highlight how the two-step mechanism can advantageously funnel energy from multiple materials to a single charge-generating interface and suggest a route to new-concept devices.

For our interlayer thickness dependence study, we have focused on two, well-characterized donor/acceptor couples: P3HT/C_{60} and CuPc/C_{60}. Previous studies have indicated that P3HT/C_{60} relies on the two-step process while CuPc, which does not readily transfer energy to C_{60}, does not.[30] As such, we employ CuPc/C_{60} as a control system. In an attempt to deduce the effective range of the energy transfer step in the two-step process, we have systematically varied the thickness of a TPD electron blocking layer. The architecture for our TRMC samples includes only the active layers on quartz (quartz/CuPc/TPD/C_{60} and quartz/P3HT/TPD/C_{60}). The working device architectures include an indium−tin−oxide (ITO) anode, poly(3,4-ethylenedioxythiophene):poly(styrene sulfonate) (PEDOT:PSS) hole transport layer, a bathocuproine (BCP) exciton blocking layer to help prevent shorting, and a silver cathode (ITO/PEDOT:PSS/CuPc/TPD/C_{60}/BCP/Ag and ITO/PEDOT:PSS/P3HT/TPD/C_{60}/BCP/Ag). On the basis of its energy levels (Figure 1a), the TPD layer should (1) disrupt electron transfer from P3HT to C_{60} and from CuPc to C_{60}, (2) permit hole transfer from C_{60} to P3HT and from C_{60} to CuPc. Fabrication details are given in the Methods section.

Figure 1c shows the EQEs of CuPc/TPD/C_{60} devices as the TPD layer thickness is varied from 0 to 9 nm. With no TPD, the action spectrum exhibits the absorption peaks of C_{60} (~450 nm) and CuPc (620 and 700 nm). As the TPD thickness is increased to 4 nm, the contribution to the action spectrum from CuPc absorption

is significantly reduced while the C_{60} absorption contribution remains. These data are consistent with the interpretation that the TPD layer prevents electron transfer from CuPc to C_{60} but allows exciton (C_{60}*) dissociation and hole transfer from C_{60} to TPD to CuPc.

Figure 1d shows the EQEs of P3HT/TPD/C_{60} devices as the TPD layer thickness is varied from 0 to 50 nm. With no TPD, the action spectrum displays the absorption peak of C_{60} near 450 nm and the broader absorption of P3HT out to 650 nm. When 3 nm of TPD is inserted between P3HT/C_{60}, in contrast to the CuPc/TPD/C_{60} system, the action spectrum drops minimally. Even at a TPD thickness of 11 nm, the EQE at 600 nm is only reduced by ~50%. Only at TPD thicknesses approaching 50 nm does the action spectrum approach the shape of the C_{60} absorption spectrum. The fact that such a thick TPD layer is necessary to disrupt the P3HT/C_{60} devices, much thicker than the CuPc/C_{60} devices, suggests that the TPD blocks a different photophysical process in the P3HT/C_{60} devices than in the CuPc/C_{60} devices.

To understand the P3HT/TPD/C_{60} system fully, charge generation in the P3HT and C_{60} layers must be considered separately. In the P3HT/TPD/C_{60} devices, the contribution to the photocurrent from excitons generated in the C_{60} is mostly retained when TPD is added. Even for the thickest TPD layers, the C_{60} component is mostly retained, and indeed, the action spectra mimic the C_{60} absorption spectra. This suggests that, even with TPD, the excitons generated in the C_{60} still dissociate (*via* hole transfer to the HOMO of the TPD) and that the free holes can migrate through the TPD to the P3HT.

The story is more complicated for those excitons generated in the P3HT. The position of the TPD LUMO level (Figure 1a) would suggest that electrons generated in the P3HT should be prevented from migrating to the C_{60} except through tunneling. However, a significant P3HT component remains in the P3HT/TPD/C_{60} devices with TPD so thick as to prevent electron tunneling. Longer-range energy transfer across this barrier can explain this observation. While a more detailed analysis of this energy transfer process will be given below, these preliminary observations of the length scale of the transfer process support the proposed mechanism of the two-step process: excitons generated in the P3HT energy transfer across the TPD, with subsequent hole transfer back from the C_{60} to the P3HT. The efficacy of this process is only limited by the ability of the excitons to cross the TPD barrier, exciton dissociation at the TPD/C_{60} interface, and subsequent hole transport through the TPD.

To confirm that the TPD layer is indeed blocking electron transfer, we have performed a number of control experiments. Of primary importance is the quality and continuity of the TPD interfacial layer. Proving indisputably that the TPD layer is continuous and that the evaporated C_{60} does not penetrate across the TPD barrier is beyond the scope of this article. However, several observations and experiments lead us to believe that the TPD layer is truly separating the C_{60} and P3HT. First, it is worth noting that 4 nm of TPD successfully

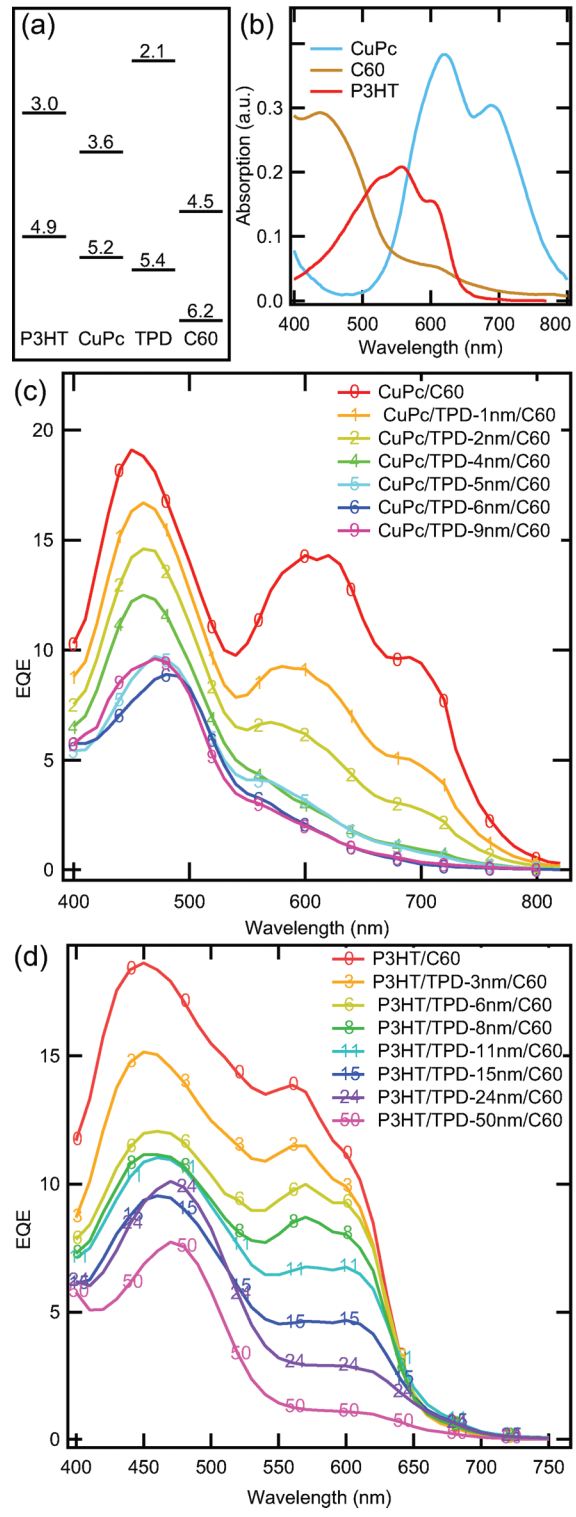

Figure 1. (a) Energy levels in electronvolts of P3HT, CuPc, TPD, and C_{60}.[30] (b) Absorption spectra of CuPc, C_{60}, and P3HT. (c) Action spectra of CuPc/TPD/C_{60} devices for varying TPD thickness (0, 1, 2, 4, 5, 6, 9 nm). (d) Action spectra of P3HT/TPD/C_{60} devices for varying TPD thickness (0, 3, 6, 8, 11, 15, 24, 50 nm).

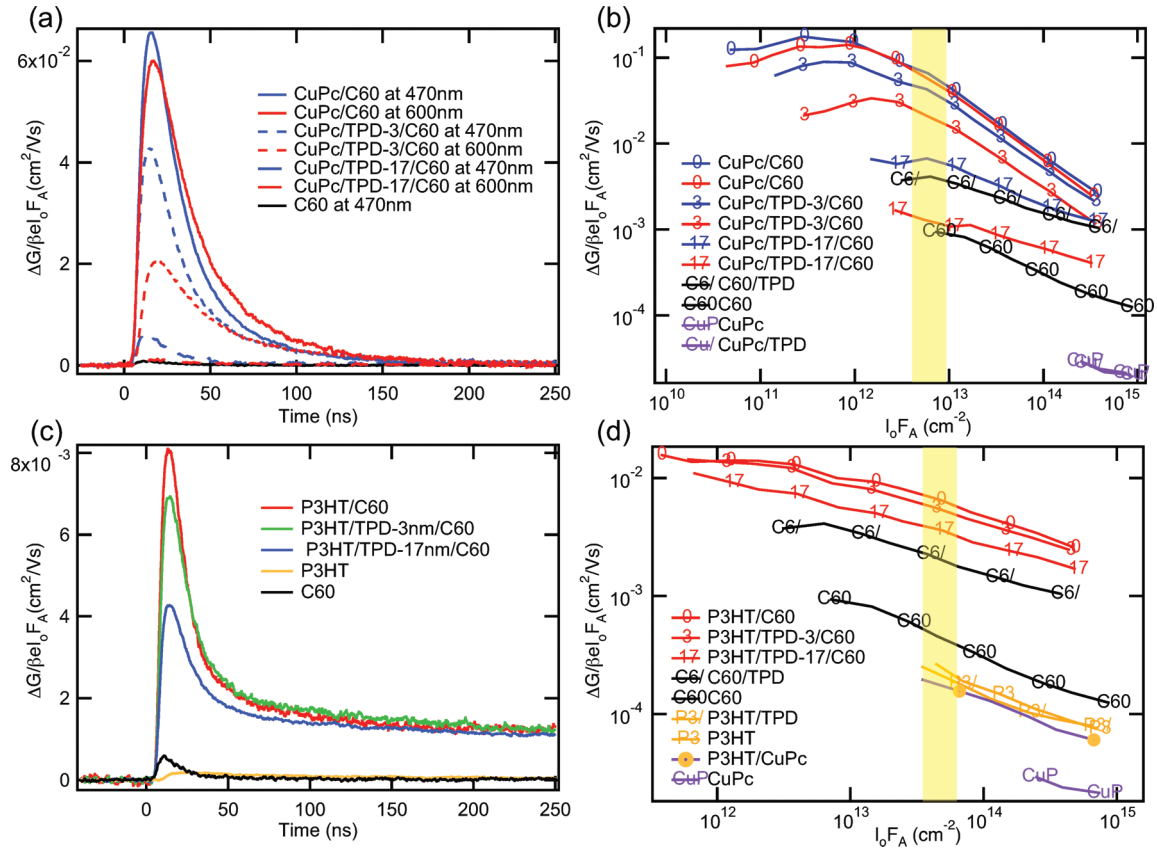

Figure 2. (a) TRMC photoconductance transients and (b) peak photoconductance signals of the CuPc/TPD/C_{60} system. Trilayer data were acquired at 470 nm (blue traces) and at 600 nm (red traces) for TPD thicknesses of 0, 3, and 17 nm. C_{60} and TPD/C_{60} data (black traces) were collected at 470 nm. CuPc and CuPc/TPD data (purple traces) were collected at 600 nm. (c) TRMC photoconductance transients and (d) peak photoconductance signals of the P3HT/TPD/C_{60} system collected at 600 nm. Trilayer data were collected for TPD thicknesses of 0, 3, and 17 nm and are compared to C_{60} and C_{60}/TPD data (black traces), P3HT and P3HT/TPD data (orange traces), and P3HT/CuPc (orange/purple trace). The traces shown in (a) and (c) correspond to the intensity denoted in (b) and (d) by the yellow bars. All data are normalized by the corresponding sample's wavelength-specific absorbance.

blocks electron transfer in the CuPc/TPD/C_{60} system, hence any TPD pin-holes or C_{60} interpenetration would be specific of the P3HT/TPD processing and not an inherent feature of TPD. Second, using intermittent-contact AFM, we measure a rms roughness of our P3HT and CuPc samples at 1.7 and 3.8 nm, respectively, suggesting that our thicker TPD layers should form a conformal layer. Third, we have fabricated P3HT/BCP/C_{60} devices, where 3 nm of BCP, a transparent wide band gap small-molecule, fully blocks hole and electron transfer, which shows that a thin layer of evaporated small molecules can block charge transfer despite the potential of interpenetration into the softer P3HT. Fourth, we have fabricated inverted devices and see similar TPD trends to those in Figure 1 for both CuPc and P3HT systems.

Most importantly, we have performed a series of complementary TRMC experiments. TRMC allows us to probe the charge-generating performance of active layer materials while avoiding the complicating factors associated with the anode, cathode, PEDOT, and BCP layers comprising a full device. Additionally, TRMC can compare pure materials or bilayers, such as P3HT/TPD, that fail to perform in photovoltaic devices. TRMC measurements were carried out on an apparatus described elsewhere.[26,32−34] Briefly, with a sample placed in the TRMC resonant microwave chamber, the transient change in microwave power, ΔP, due to a 5 ns, adjustable-wavelength laser pulse is proportional to the transient change in the sample's photoconductance, ΔG. $\Delta P(t)/P = -K\Delta G(t)$, where K is a "sensitivity factor" that can be calculated from the dimensions of the microwave cavity and the sample dielectric properties. With TRMC, we are able to address the following questions: (1) Is free charge being generated at the P3HT/TPD or the CuPc/TPD interfaces? (2) Is free charge being generated at C_{60}/TPD interfaces? (3) Is TPD preventing charge generation or simply blocking charge transport and extraction?

Figure 2 shows TRMC photoconductance data, $\Delta G/\beta e I_0 F_A$, where ΔG is the change in photoconductance, β is the ratio between the long and short distances of the waveguide, I_0 is the incident photon flux, and F_A is the wavelength-specific fraction of light absorbed. To first-order, the peak magnitudes of $\Delta G/\beta e I_0 F_A$ indicate the photoconductance, which,

as discussed below, is an indication of the number of charges generated.

Figure 2a plots example photoconductance traces taken for the CuPc/TPD/C_{60} system, with each trace being normalized by its wavelength-specific absorption. Data were acquired while exciting at 470 nm (blue traces), where CuPc absorbs little, and at 600 nm (red traces), where C_{60} absorbs little. Figure 2b shows the dependence of the peak value of such transients with intensity. The illumination intensity used for the traces in Figure 2a is represented by the yellow bar in Figure 2b.

Several observations can be made from these data. First, the relatively low photoconductance signals seen in pure C_{60} (black trace) and CuPc (purple trace) increase by over an order of magnitude in a C_{60}/CuPc bilayer. Previous TRMC studies have shown that the TRMC photoconductance signal is proportional to the product of the number of charges and their mobility, and that a photoconductance signal that is higher in a bilayer than in each of the individual layers is an indication of charge generation at the interface.[26,32−34] As such, we attribute the increased photoconductance to an increase in charge generation (we will continue to use this interpretation in all subsequent data). Second, the CuPc/TPD signal is nearly identical to the CuPc-only signal, while the C_{60}/TPD signal is higher than the C_{60}-only signal. This observation indicates that the C_{60}/TPD interface is a charge-generating interface while the CuPc/TPD interface is not. Third, with 3 nm TPD interlayers in CuPc/TPD/C_{60}, the signal at low light intensity in Figure 2b drops by 40% with excitation at 470 nm and by 78% with excitation at 600 nm. These drops compare similarly to the drops measured in the full devices shown in Figure 1c (drops of 32 and 79% for 4 nm TPD). Given that TRMC probes charge generation and not charge transport/extraction, the agreement between the TRMC data of electrodeless "devices" and EQE data for working devices indicates that the reduction in efficiency associated with a TPD interfacial layer in full devices is due to a reduction in free charge generation.

Figure 2c,d plots, respectively, the TRMC photoconductance transients and the peak values of such transients for the P3HT/TPD/C_{60} system. The P3HT and P3HT/C_{60} traces are shown at 600 nm excitation where P3HT absorption dominates. Several observations can be made. First, the relatively low signals seen in pure P3HT and pure C_{60} increase by over an order of magnitude when they are combined into a bilayer. Again, we interpret this as confirmation that TRMC can be used to observe the expected charge-generation ability of the P3HT/C_{60} interface. Second, the P3HT/TPD signal is nearly identical to the pure P3HT signal, indicating that the P3HT/TPD interface is not a charge-generating interface (again, the C_{60}/TPD interface *is* charge-generating). Third, with 3 and 17 nm TPD interlayers, the signal decreases by 10 and 50%, respectively. This drop is much less than the TRMC signal drop in the CuPc/TPD/C_{60} system and is again consistent with the P3HT system full device data. These TRMC data support the interpretation that the TPD interface blocks electron transfer from the P3HT, but somehow the excitons absorbed in the P3HT are still able to dissociate into free charge—presumably through the two-step process.

Having provided further evidence that the two-step process can occur in P3HT/C_{60}, we return to a more detailed analysis of the data in Figure 1d, which characterizes the length scale of the two-step process. At 600 nm, the EQE of P3HT/TPD/C_{60} devices drops 17, 40, 74, and 90% for TPD thicknesses of 6, 11, 24, and 50 nm, respectively. The fact that devices continue to generate photocurrent with such thick blocking layers is inconsistent with an electron tunneling mechanism but consistent with long-range energy transfer.

Energy transfer is typically described by Dexter, Förster, or radiative mechanisms.[15,19] The TPD barrier thickness through which the energy can successfully hop in a single jump is too large to be accounted for by Dexter energy transfer (which typically operates at less than 0.5 nm)[19] but is shorter than would be expected for efficient radiative transfer (greater than 1 μm for TPD, which is transparent in the visible). The radiative mechanism is also unlikely given the poor photoluminescence quantum yield (PLQY) of P3HT and poor optical absorption of C_{60}.

To understand how the FRET mechanism can be used to describe the data in Figure 1d, we first begin with a basic discussion of FRET and proceed to describe how this traditional description must be modified to understand our trilayer structures. In the standard, simplified description of FRET, the exciton is presumed to jump from a single, isolated emitter dipole to a single, isolated absorber dipole within a homogeneous dielectric medium.[1,15,19] For sufficiently long jumps satisfying the mathematical approximation of a dipole−dipole transition, $\kappa\tau = (R_0/R)^6$, where κ is the FRET rate, τ is the exciton lifetime, and R_0 is the Förster radius. It is worth noting that the R_0 is fundamentally different to an exciton diffusion length, which incorporates multiple hopping events undergoing a random walk.

The FRET rate is derived to be proportional to the PLQY of the donor and the spectral overlap of the donor emission and acceptor absorption. This rate would be expected, upon first examination, to be relatively small for the P3HT/C_{60} system, as their spectral overlap is small and the PLQY of P3HT is low (note, though, that any decrease in R_0 is accordingly smaller given the 1/6th power functional relationship between the rate and R_0). However, the simple description of FRET given above must be expanded to accurately represent our layered architectures. First, the dipole−dipole approximation is not satisfied by our trilayer device geometry, where one would expect transfer to occur from a single donor chromophore dipole to any of a number of chro-

mophores in the acceptor layer. This difference in geometry from a dipole−dipole transfer to dipole−slab transfer has been shown by several groups to alter the traditional transfer rate from the $1/R^6$ distance dependence to $1/R^3$, increasing the range of FRET.[31,35,36]

For the P3HT/TPD/C_{60} system, a standard calculation of the Förster radius using a dipole−dipole approximation[19,37] gives $R_0 = \sim 3.0$ nm for $\kappa\tau = (R_0/R)^6$ (using an experimentally measured C_{60} absorption spectrum, an experimentally measured P3HT fluorescence spectrum, and a P3HT PLQY of 0.02[38]). To more accurately describe our system, we have used a dipole−infinite-slab approximation (assuming that the overall FRET rate is the sum of all the individual FRET rates between the donor and slab of acceptors) following the method of Scully *et al.*[35] and calculated a R_0 of $\sim$9 nm for $\kappa\tau = (R_0/R)^3$. While this simplest calculation assumes that the dipoles do not perturb each other, a R_0 of 9 nm is consistent with Figure 1d. Thus, the data in Figure 1d support the interpretation that our P3HT/C_{60} devices are operating by means of long-range FRET.

Extracting quantitative FRET rates from such data requires a more detailed level of simulation, which is a future direction of our work. The dipole−slab geometry, though an improvement over the dipole−dipole geometry, is still an assumption that does not fully describe a real trilayer system or a bulk heterojunction device. In a real system, excitons can diffuse through the donor material before undergoing FRET to an acceptor. Second, if there is coherence between the multiple acceptors, then the FRET rate will be additionally modified.[39] Equally important when considering such data is that a measured EQE is not necessarily a perfect indication of an underlying FRET rate.

In these experiments, we have taken care that our devices are limited primarily by energy transfer—and not by diffusion, dissociation, or charge transport. As such, while there is no perfect comparison available between our data and an analysis of dipole−dipole systems or bulk heterojunction systems, our trilayer devices provide a good qualitative example of how, to first-order, energy transfer proceeds in standard OPVs.

Regardless of the theoretical interpretation, it is still intriguing that the FRET length scales we measure, which are due to single hops, are comparable to the exciton diffusion lengths commonly measured for P3HT, which are based on multiple hops. The exciton diffusion length in P3HT has been measured in a variety of experiments, with results generally between 5 and 15 nm.[10−13] This range is similar to the P3HT domain sizes measured by TEM for optimized bulk heterojunction P3HT/PCBM devices as well as the thicknesses employed for optimized P3HT/C_{60} planar devices.[40,41] This agreement has traditionally been used as proof for the hypothesis that devices are optimized such that the multihop diffusion ensures excitons reach donor/acceptor interfaces. However, the similar range we measure for the two-step process presents the possibility that P3HT−fullerene devices have been morphologically optimized to maximize two-step energy transfer from P3HT to an acceptor, and that single hops from donor to acceptor could be dominating the range over which energy transfer occurs. While this mechanism cannot describe charge generation in all donor/acceptor systems (some acceptors have wider band gaps than the corresponding donors), it suggests that a new strategy for improving charge generation in some organic photovoltaic cells would be to enhance long-range FRET from donor materials to acceptor materials.

Beyond showing that a two-step charge-generation process based on long-range FRET is an important factor in the operation of P3HT/C_{60} devices, we now provide an example of how this two-step process can be used to supplement device efficiency. In the P3HT/TPD/C_{60} devices previously discussed, the thin TPD layers do not significantly reduce performance, but they do not benefit the devices and thus there is an overall performance loss. If, however, we replace the TPD with a material that still allows hole transfer yet absorbs visible light, it becomes possible to increase the overall device performance. Figure 3 shows the EQEs of a series of such devices with P3HT/CuPc/C_{60} active layers. In these trilayer devices, the P3HT and C_{60} thicknesses were held constant at 30 and 50 nm, while the CuPc thickness was varied at 2, 5, and 7 nm. Figure 3 compares the EQE of these trilayer devices (green traces) to P3HT/C_{60} bilayer devices (red traces) and CuPc/C_{60} bilayer devices (blue traces).

Figure 3a compares the EQE data for the 2 nm CuPc system: P3HT/CuPc-2 nm/C_{60}, CuPc-2 nm/C_{60}, and P3HT/C_{60} devices. The trilayer device gives enhanced performance in the red compared to the P3HT/C_{60} bilayer device, showing that CuPc absorbance is contributing to device efficiency. Significantly, the efficiency of the trilayer device in the blue is little less than that of the P3HT/C_{60} bilayer device. This minimal loss in the blue is what was observed for P3HT/TPD/C_{60} devices in Figure 2d for thin TPD layers and is suggestive of the two-step mechanism operating in the P3HT/CuPc/C_{60} system. Figure 3b,c shows analogous EQE data as the CuPc layer is increased to 5 and 7 nm, respectively. As the CuPc layer thickness is increased, the trilayer device efficiencies increase in the red where CuPc correspondingly absorbs. However, a second trend is that the performance in the green, where P3HT absorbs, begins to decrease—presumably as the excitons generated in the P3HT are unable to FRET transfer to the C_{60}. Compared to 2 nm CuPc and 7 nm CuPc, the 5 nm CuPc gives an optimal balance of increased absorption in the red and reduced energy transfer from P3HT. Importantly, the P3HT/CuPc-5 nm/C_{60} device (uncertified solar power conversation efficiency, $\eta = 1.12\%$) is more efficient than either of the P3HT/CuPc-2 nm/C_{60} (0.72%) or P3HT/CuPc-7 nm/C_{60} (0.98%) trilayer devices and is more effi-

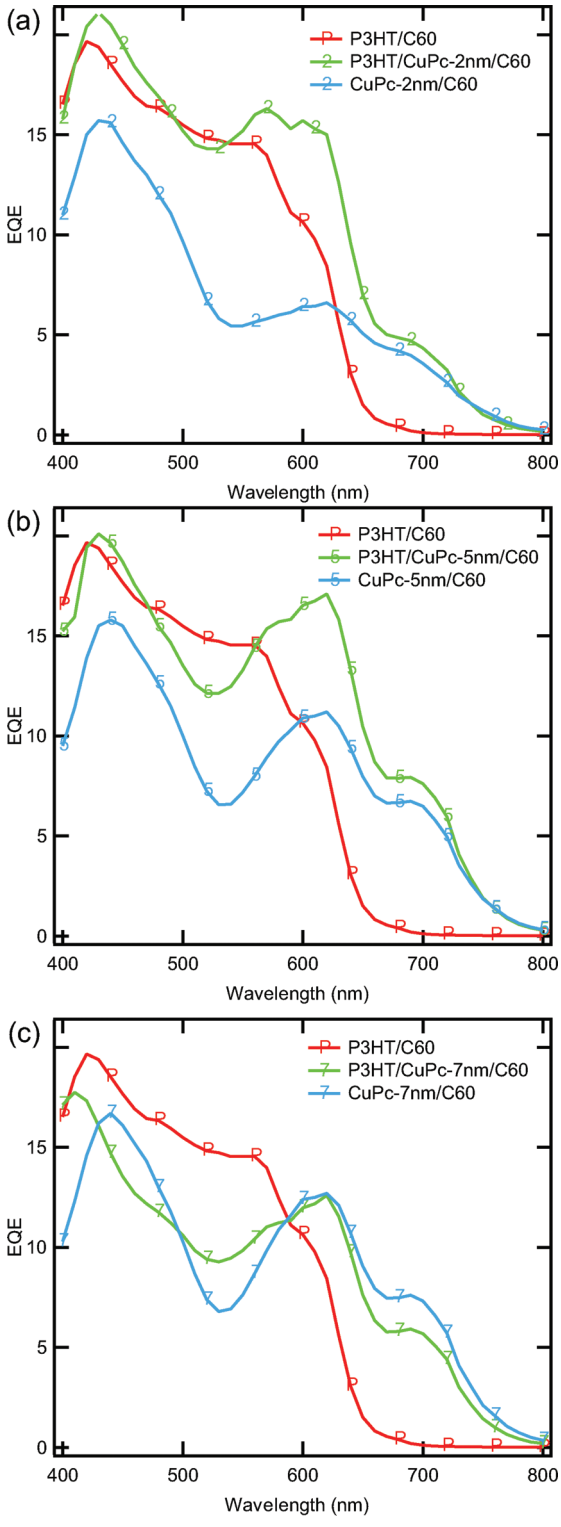

Figure 3. EQE spectra of P3HT-30 nm/CuPc/C_{60}-50 nm devices (green traces) compared to P3HT-30 nm/C_{60}-50 nm devices (red traces) and CuPc/C_{60}-50 nm devices (blue traces) for CuPc thickness of (a) 2, (b) 5, and (c) 7 nm.

cient than the P3HT/C_{60} (0.57%) and CuPc-5 nm/C_{60} (0.60%) bilayer devices.

As further confirmation that the two-step charge-generation process occurs in P3HT/CuPc/C_{60} devices, we have again employed TRMC. Figure 2d compares the TRMC signal in a P3HT/CuPc bilayer (purple/orange trace) to a pure P3HT film (orange trace). Significantly, the P3HT/CuPc bilayer does not show any increase in charge generation compared to a pure P3HT film. This suggests that charge is not readily generated at P3HT/CuPc interfaces. Correspondingly, we note that simple P3HT/CuPc bilayer devices are not reported in the literature (the P3HT/CuPc bilayer devices we have attempted give no short-circuit current and very low shunt resistance). CuPc/P3HT:PCBM solar cells have been demonstrated, but in these cells, both the CuPc and P3HT contact PCBM and it can be presumed that the CuPc/PCBM and P3HT/PCBM channels operate in parallel.[8] As such, we conclude that, within P3HT/CuPc/C_{60} devices, the CuPc/C_{60} interface is the only efficient charge-generating interface. Those excitons photogenerated in the P3HT must transfer energy, using FRET, across the CuPc layer to the C_{60}. It is possible that this transfer could occur by way of diffusion through the CuPc, though given the similarities to the P3HT/TPD/C_{60} system the two-step process seems more likely. Either way, energy is being funneled from multiple materials to a single charge-generation interface. This is in contrast to standard multilayer devices such as tandem solar cells where multiple charge-generating interfaces operate in series. The EQE data for the trilayer devices shown in Figure 3, however, most likely achieve their higher performance by employing the two-step mechanism.

CONCLUSION

In conclusion, we have shown that a two-step charge-generation process can play an important role in the operation, understanding, and improvement of certain organic photovoltaics. By testing the length scale over which this two-step mechanism can proceed, we have shown that the energy transfer step in the two-step mechanism relies on Förster resonance energy transfer (FRET). Further, the FRET operates over surprisingly long length scales dependent on the sample architecture/morphology, which presents an intriguing new pathway of moving energy over the distances necessary for the next generation of organic photovoltaics. Materials with more efficient FRET than P3HT could significantly enhance device efficiency. Finally, we have fabricated trilayer devices that provide an example of how this two-step mechanism can be used to supplement OPV efficiency. These P3HT/CuPc/C_{60}-based solar cells demonstrate improved efficiency compared to traditional bilayer devices. However, the key to this performance boost is not based on the mechanism found in traditional tandem cells where multiple charge-generating interfaces operate in series, but rather through the two-step mechanism shuttling energy from multiple materials to a single charge-

generating interface. We envision that future devices designed to fully incorporate the advantages of the two-step mechanism might provide enhanced long-range energy transfer and performance.

METHODS

Device Fabrication: Current−voltage and EQE measurements were carried out on 0.11 cm^2 photovoltaic cells. These devices were fabricated on prepatterned indium−tin−oxide (ITO)-coated glass substrates cleaned by sonication in deionized water, acetone, and isopropyl alcohol, followed by a 5 min oxygen plasma treatment. The active layers were deposited as follows: first PEDOT:PSS (Clevios P VP Al 4083) layer was spin-coated at 4000 rpm, then annealed at 130 °C for 15 min. P3HT solutions (Rieke Metals Inc., 5 mg/mL in chlorobenzene) were spin-coated at 2500 rpm. CuPc (20 nm, Aldrich), TPD (Aldrich), and C_{60} (50 nm, Nano-C) were deposited under vacuum ($<5 \times 10^{-6}$ Torr) at rates of 0.5, 0.3, and 1 Å/s, respectively. Six nanometers of BCP (Aldrich) was deposited at a rate of 0.5 Å/s before deposition of a 100 nm silver cathode, which was evaporated under vacuum ($<2 \times 10^{-7}$ Torr) at a rate of 2 Å/s.

Bulk Device Characterization: Device measurements were made in a nitrogen environment. Efficiency measurements were taken under an average full-spectrum intensity of 1000 W/m^2 as describe in ref 42. EQEs were calculated by taking the ratio of the device photocurrent to the corrected photocurrent of a Si photodiode with a calibrated spectral response.

TRMC Sample Characterization: TRMC samples were prepared on quartz substrates without electrodes or charge transport layers (without ITO anode, PEDOT:PSS, BCP, or Ag). The active layers were prepared identically to the full devices, except that the C_{60} thickness was set at 30 nm. TRMC measurements were carried out on an apparatus described elsewhere.[26,32−34] The TRMC data are normalized by the wavelength-specific absorption of each sample. The absorption data were measured using a UV−vis spectrophotometer equipped with an integrating sphere (Shimadzu UV-3600).

Acknowledgment. We gratefully acknowledge Ross Larsen and Matthew Lloyd for valuable insight and discussion, and the Gregg lab for assistance making devices. This work was funded by the Solar Photochemistry program of the U.S. Department of Energy, Office of Science, Basic Energy Sciences, Division of Chemical Sciences, Geosciences and Biosciences, under Contract No. DE-AC36-08-GO28308 to NREL.

REFERENCES AND NOTES

1. Gregg, B. A. The Photoconversion Mechanism of Excitonic Solar Cells. *MRS Bull.* **2005**, *30*, 20–22.
2. Nelson, J. Solar Energy—Solar Cells by Self-Assembly. *Science* **2001**, *293*, 1059–1060.
3. Barker, J. A.; Ramsdale, C. M.; Greenham, N. C. Modeling the Current−Voltage Characteristics of Bilayer Polymer Photovoltaic Devices. *Phys. Rev. B* **2003**, *67*, 075205-1–075205-9.
4. Ayzner, A. L.; Tassone, C. J.; Tolbert, S. H.; Schwartz, B. J. Reappraising the Need for Bulk Heterojunctions in Polymer−Fullerene Photovoltaics: The Role of Carrier Transport in All-Solution-Processed P3ht/Pcbm Bilayer Solar Cells. *J. Phys. Chem. C* **2009**, *113*, 20050–20060.
5. Hardin, B. E.; Hoke, E. T.; Armstrong, P. B.; Yum, J.; Comte, P.; Torres, T.; Frechet; Nazeeruddin, M. K.; Graetzel, M.; McGehee, M. D. Increased Light Harvesting in Dye-Sensitized Solar Cells with Energy Relay Dyes. *Nat. Photonics* **2009**, *3*, 406–411.
6. Liu, Y. X.; Summers, M. A.; Edder, C.; Frechet, J. M. J.; McGehee, M. D. Using Resonance Energy Transfer To Improve Exciton Harvesting in Organic−Inorganic Hybrid Photovoltaic Cells. *Adv. Mater.* **2005**, *17*, 2960–2964.
7. Liu, Y. X.; Summers, M. A.; Scully, S. R.; McGehee, M. D. Resonance Energy Transfer from Organic Chromophores to Fullerene Molecules. *J. Appl. Phys.* **2006**, *99*, 093521-1–093521-4.
8. Ohkita, H.; Cook, S.; Astuti, Y.; Duffy, W.; Tierney, S.; Zhang, W.; Heeney, M.; McCulloch, L.; Nelson, J.; Bradley, D. C.; Durrant, J. R. Charge Carrier Formation in Polythiophene/Fullerene Blend Films Studied by Transient Absorption Spectroscopy. *J. Am. Chem. Soc.* **2008**, *130*, 3030–3042.
9. Muntwiler, M.; Yang, Q.; Tisdale, W. A.; Zhu, X. Coulomb Barrier for Charge Separation at an Organic Semiconductor Interface. *Phys. Rev. Lett.* **2008**, *101*, 196403-1–196403-4.
10. Halls, J. J. M.; Pichler, K.; Friend, R. H.; Moratti, S. C.; Holmes, A. B. Exciton Diffusion and Dissociation in a Poly(*p*-phenylenevinylene)/C-60 Heterojunction Photovoltaic Cell. *Appl. Phys. Lett.* **1996**, *68*, 3120–3122.
11. Haugeneder, A.; Neges, M.; Kallinger, C.; Spirkl, W.; Lemmer, U.; Feldmann, J.; Scherf, S.; Harth, E.; Gugel, A.; Mullen, K. Exciton Diffusion and Dissociation in Conjugated Polymer Fullerene Blends and Heterostructures. *Phys. Rev. B* **1999**, *59*, 15346–15351.
12. Markov, D. E.; Amsterdam, E.; Blom, P. W. M.; Sieval, A. B.; Hummelen, J. C. Accurate Measurement of the Exciton Diffusion Length in a Conjugated Polymer Using a Heterostructure with a Side-Chain Cross-Linked Fullerene Layer. *J. Phys. Chem. A* **2005**, *109*, 5266–5274.
13. Theander, M.; Yartsev, A.; Zigmantas, D.; Sundstrom, V.; Mammo, W.; Andersson, M. R.; Inganas, O. Photoluminescence Quenching at a Polythiophene/C-60 Heterojunction. *Phys. Rev. B* **2000**, *61*, 12957–12963.
14. Shaheen, S. E.; Brabec, C. J.; Sariciftci, N. S.; Padinger, F.; Fromherz, T.; Hummelen, J. C. 2.5% Efficient Organic Plastic Solar Cells. *Appl. Phys. Lett.* **2001**, *78*, 841–843.
15. Beljonne, D.; Curutchet, C.; Scholes, G. D.; Silbey, R. J. Beyond Forster Resonance Energy Transfer in Biological and Nanoscale Systems. *J. Phys. Chem. B* **2009**, *113*, 6583–6599.
16. Bredas, J. L.; Beljonne, D.; Coropceanu, V.; Cornil, J. Charge-Transfer and Energy-Transfer Processes in π-Conjugated Oligomers and Polymers: A Molecular Picture. *Chem. Rev.* **2004**, *104*, 4971–5003.
17. Gregg, B. A.; Sprague, J.; Peterson, M. W. Long-Range Singlet Energy Transfer in Perylene Bis(phenethylimide) Films. *J. Phys. Chem. B* **1997**, *101*, 5362–5369.
18. Madigan, C.; Bulovic, V. Modeling of Exciton Diffusion in Amorphous Organic Thin Films. *Phys. Rev. Lett.* **2006**, *96*, 046404-1–046404-4.
19. Scholes, G. D. Long-Range Resonance Energy Transfer in Molecular Systems. *Annu. Rev. Phys. Chem.* **2003**, *54*, 57–87.
20. Krause, G. H.; Weis, E. Chlorophyll Fluorescence and Photosynthesis—The Basics. *Annu. Rev. Plant Phys.* **1991**, *42*, 313–349.
21. Nelson, N.; Ben-Shem, A. The Complex Architecture of Oxygenic Photosynthesis (Vol. 5, p 971, 2004). *Nat. Rev. Mol. Cell. Biol.* **2005**, *6*, 818.
22. Chen, H.; Hou, J.; Zhang, S.; Liang; Yang, G.; Yang, Y.; Yu, L.; Wu, Y.; Li, G. Polymer Solar Cells with Enhanced Open-Circuit Voltage and Efficiency. *Nat. Photonics* **2009**, *3*, 649–653.
23. Park, S. H.; Roy, A.; Beaupre, S.; Cho, S.; Coates, N.; Moon, J. S.; Moses, D.; Leclerc, M.; Lee, K.; Heeger, A. J. Bulk Heterojunction Solar Cells with Internal Quantum Efficiency Approaching 100%. *Nat. Photonics* **2009**, *3*, 297–303.
24. Athanasopoulos, S.; Hennebicq, E.; Beljonne, D.; Walker, A. B. Trap Limited Exciton Transport in Conjugated Polymers. *J. Phys. Chem. C* **2008**, *112*, 11532–11538.
25. Brabec, C. J.; Zerza, G.; Cerullo, G.; De Silvestri, S.; Luzzati, S.; Hummelen, J. C.; Sariciftci, S. Tracing Photoinduced Electron Transfer Process in Conjugated Polymer/Fullerene

Bulk Heterojunctions in Real Time. *Chem. Phys. Lett.* **2001**, *340*, 232–236.
26. Dicker, G.; de Haas, M. P.; Siebbeles, L. D. A.; Warman, J. M. Electrodeless Time-Resolved Microwave Conductivity Study of Charge-Carrier Photogeneration in Regioregular Poly(3-hexylthiophene) Thin Films. *Phys. Rev. B* **2004**, *70*, 045203-1–045203-8.
27. Sheng, C.; Tong, M.; Singh, S.; Vardeny, Z. V. Experimental Determination of the Charge/Neutral Branching Ratio η in the Photoexcitation of π-Conjugated Polymers by Broadband Ultrafast Spectroscopy. *Phys. Rev. B* **2007**, *75*, 085206-1–085206-7.
28. Rothburg, L. J.; Yan, M.; Papadimitrakopoulos, F.; Galvin, M. E.; Kwock, E. W.; Miller, T. M. Photophysics of Phenylenevinylene Polymers. *Synth. Met.* **1996**, *80*, 41–58.
29. Schueppel, R.; Uhrich, C.; Pfeiffer, M.; Leo, K.; Brier, E.; Reinold, E.; Baeuerle, P. Enhanced Photogeneration of Triplet Excitons in an Oligothiophene−Fullerene Blend. *ChemPhysChem* **2007**, *8*, 1497–1503.
30. Lloyd, M. T.; Lim, Y.; Malliaras, G. G. Two-Step Exciton Dissociation in Poly(3-hexylthiophene)/Fullerene Heterojunctions. *Appl. Phys. Lett.* **2008**, *92*, 143308-1–143308-3.
31. Shaw, P. E.; Ruseckas, A.; Samuel, I. D. W. Distance Dependence of Excitation Energy Transfer between Spacer-Separated Conjugated Polymer Films. *Phys. Rev. B* **2008**, *78*, 245201-1–245201-5.
32. Kroeze, J. E.; Savenije, T. J.; Vermeulen, M. J. W.; Warman, J. M. Contactless Determination of the Photoconductivity Action Spectrum, Exciton Diffusion Length, and Charge Separation Efficiency in Polythiophene-Sensitized TiO_2 Bilayers. *J. Phys. Chem. B* **2003**, *107*, 7696–7705.
33. Piris, J.; Kopidakis, N.; Olson, D. C.; Shaheen, S. E.; Ginley, D. S.; Rumbles, G. The Locus of Free Charge-Carrier Generation in Solution-Cast Zn1-Xmgxo/Poly(3-hexylthiophene) Bilayers for Photovoltaic Applications. *Adv. Funct. Mater.* **2007**, *17*, 3849–3857.
34. Ferguson, A. J.; Kopidakis, N.; Shaheen, S. E.; Rumbles, G. Quenching of Excitons by Holes in Poly(3-hexylthiophene) Films. *J. Phys. Chem. C* **2008**, *112*, 9865–9871.
35. Scully, S. R.; Armstrong, P. B.; Edder, C.; Frechet, M. J.; Mcgehee, M. D. Long-Range Resonant Energy Transfer for Enhanced Exciton Harvesting for Organic Solar Cells. *Adv. Mater.* **2007**, *19*, 2961–2966.
36. Scully, S. R.; Mcgehee, M. D. Effects of Optical Interference and Energy Transfer on Exciton Diffusion Length Measurements in Organic Semiconductors. *J. Appl. Phys.* **2006**, *100*, 034907-1–034907-5.
37. Forster, T. *Discuss. Faraday Soc.* **1959**, *27*, 7–17.
38. Cook, S.; Furube, A.; Katoh, R. Analysis of the Excited States of Regioregular Polythiophene P3ht. *Energy Environ. Sci.* **2008**, *1*, 294–299.
39. Collini, E.; Wong, C. Y.; Wilk, K. E.; Curmi, P. M. G.; Brumer, P.; Scholes, G. D. Coherently Wired Light-Harvesting in Photosynthetic Marine Algae at Ambient Temperature. *Nature* **2010**, *463*, 644–649.
40. Savenije, T. J.; Kroeze, J. E.; Yang, X. N.; Loos, J. The Effect of Thermal Treatment on the Morphology and Charge Carrier Dynamics in a Polythiophene-Fullerene Bulk Heterojunction. *Adv. Funct. Mater.* **2005**, *15*, 1260–1266.
41. Vanlaeke, P.; Swinnen, A.; Haeldermans, I.; Vanhoyland, G.; Aernouts, T.; Cheyns, D.; Deibel, C.; D'Haen, J.; Heremans, P.; Poortmans, J.; Manca, J. V. P3ht/Pcbm Bulk Heterojunction Solar Cells: Relation between Morphology and Electro-Optical Characteristics. *Sol. Energy Mater. Sol. Cells* **2006**, *90*, 2150–2158.
42. Reese, M. O.; White, M. S.; Rumbles, G.; Ginley, D. S.; Shaheen, S. E. Optimal Negative Electrodes for Poly(3-hexylthiophene):[6,6]-Phenyl C61-Butyric Acid Methyl Ester Bulk Heterojunction Photovoltaic Devices. *Appl. Phys. Lett.* **2008**, *92*, 053307-1–053307-5.